Phase diagram and string-density plateau state of the anisotropic triangular antiferromagnetic Ising model

2007 J. Phys.: Condens. Matter 19 145236

(http://iopscience.iop.org/0953-8984/19/14/145236)

IOP PUBLISHING JOURNAL OF PHYSICS: CONDENSED MATTER

J. Phys.: Condens. Matter **19** (2007) 145236 (6pp) doi:10.1088/0953-8984/19/14/145236

Phase diagram and string-density plateau state of the anisotropic triangular antiferromagnetic Ising model

Hiromi Otsuka[1], **Yutaka Okabe**[1] **and Kouichi Okunishi**[2]

[1] Department of Physics, Tokyo Metropolitan University, Tokyo 192-0397, Japan
[2] Department of Physics, Niigata University, Niigata 950-2181, Japan

E-mail: otsuka@phys.metro-u.ac.jp

Received 13 August 2006
Published 23 March 2007
Online at stacks.iop.org/JPhysCM/19/145236

Abstract

We report a study on the ground states of the triangular antiferromagnetic Ising model with a spacial anisotropy in the magnetic field. By the use of the level-spectroscopy and the density-matrix renormalization-group methods, we precisely determine the field-induced Berezinskii–Kosterlitz–Thouless transition point and the Pokrovski–Talapov transition points with an anisotropic nature. Then we provide the global phase diagram of the present model.

(Some figures in this article are in colour only in the electronic version)

1. Introduction

Due to the geometric frustrations, there exist some classical spin systems possessing the macroscopic ground-state entropy. The triangular antiferromagnetic Ising model (TAFIM) with the nearest-neighbour (NN) coupling is a typical one of them [1]. Further, it was exactly proven that the correlation functions of physical quantities exhibit power-law decays in the ground state [2], so the ensemble also possesses critical properties. There is a long history of research on various perturbation effects on this ground-state criticality, where some exact mappings to the triangular Ising solid-on-solid model and the fully packed loop model on the dual lattice, etc, have been utilized [3–7]. Among them, the string representation based on the fact that the ground-state spin configurations can be classified according to the number of strings (see below) provides an intuitive connection to one-dimensional (1D) quantum systems under the path-integral representation [3].

We study an anisotropic TAFIM in a magnetic field. The reduced Hamiltonian is

$$\mathcal{H}(K_1, \mu, H) = \sum_{\langle j,k \rangle} K_{jk}\delta_{\sigma_j,\sigma_k} - H\sum_j \delta_{\sigma_j,0}. \tag{1}$$

The binary variable $\sigma_j = 0, 1$ is on the jth site of the triangular lattice Λ, and the first (second) sum runs over all NN pairs (sites). The AF coupling K_{jk} takes two values $K_1 + \mu$

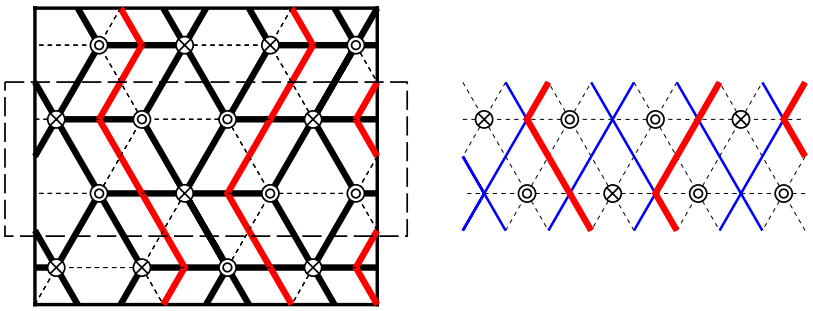

Figure 1. (a) A ground-state configuration. Dotted lines exhibit Λ; the long (short) side of the rectangle frame is in the x_1 (x_2) direction. The spins are parallel, ⊙ (antiparallel, ⊗), to the field direction. Rhombuses drawn by thick lines and three thick red lines in the x_2 direction give the tiling and the string representations, respectively. (b) A vertex representation (see section 3) of the broken-line-box region in (a).

or K_1 depending on whether the bond $\langle j, k\rangle$ lies in the x_1 direction or not (see figure 1(a)). Here, supposing that the jth site is specified by two integers (j_1, j_2), we define a quantity $Q = \sum_{j_1} N_{j_1,j_2}$ with $N_{j_1,j_2} = 1 - \delta_{\sigma_{j_1,j_2},\sigma_{j_1+1,j_2}}$ for all j_2, and further restrict ourselves to the zero temperature case $K_1 \to \infty$. Then Q becomes independent of j_2 and counts the number of strings running in the x_2 direction. The Boltzmann weight per row is given by $\mathrm{e}^{\mu Q}$, so that the anisotropy parameter μ plays the role of a chemical potential to control the number of strings (see figure 1(a)) [3].

Our main goal is to numerically obtain the phase diagram of the model (1) in its ground state $K_1 \to \infty$. For this, let us first review the effective field theoretical description on its long-distance behaviours and summarize the nature of the phase transitions. We shall start with the isotropic case $\mu = 0$. For $H = 0$, the scaling dimension of the staggered magnetization (S) is exactly given by $x_S = \frac{1}{4}$ [2], while the dimension of the uniform magnetization (s) by $x_s = \frac{9}{4}$ [4]. Thus the magnetic field is irrelevant, and the critical region continues up to a certain value H_c. For $H > H_c$, the criticality disappears and the threefold-degenerate ground state with the $\sqrt{3} \times \sqrt{3}$ structure of the sublattice is realized, where a majority spin is in the field direction. The transition at H_c is the Berezinskii–Kosterlitz–Thouless (BKT) type, and is described by the sine–Gordon Lagrangian density

$$\mathcal{L}[\phi] = \frac{1}{2\pi K}(\nabla\phi)^2 + \frac{y}{2\pi\alpha^2}\cos 3\sqrt{2}\phi, \qquad \left(K \simeq \tfrac{4}{9}\right), \tag{2}$$

where $y \propto H$ and the continuous field in the two-dimensional Euclidean space (x_1, x_2) satisfies $\sqrt{2}\phi + 2\pi = \sqrt{2}\phi$. Next, let us consider the anisotropic case $\mu \neq 0$. While the magnetic field $H > H_c$ favours the commensurate (C) ordered phase through the potential $\cos 3\sqrt{2}\phi$, μ which newly introduces a local string-density term $\partial_1\phi$ to the effective theory (2) tends to stabilize an incommensurate (IC) liquid phase [8]. Therefore, the Pokrovski–Talapov (PT) transition may occur between the C and IC phases [3, 7, 9]. Since two different types of phase transitions are expected, we employ the proper numerical methods to treat them in following sections.

2. Results in the isotropic case $\mu = 0$

There have been several attempts to numerically estimate H_c. Blöte and Nightingale (BN) investigated this problem in detail by the transfer-matrix method [5]. Actually, they evaluated

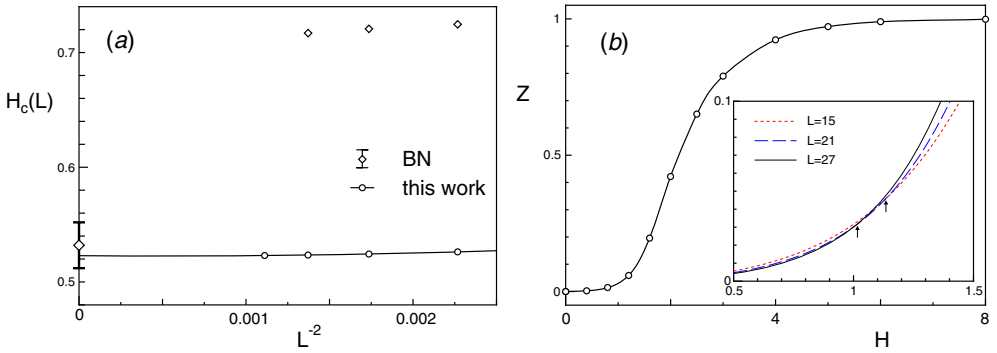

Figure 2. (a) The extrapolation of finite-size estimates (circles) to the limit $L \to \infty$. Diamonds are estimates according to the KT criterion (see the text) taken from table 1 of [5]; the one with the error bar shows BN's estimation of H_c. (b) The expectation value of the twist operator for $L = 27$. The inset shows the magnification around the transition point H_c, where the three spline fitting curves for $z(H)$ are given for $L = 15$ (red), 21 (blue), and 27 (black).

finite-size estimates $H_c(L)$ by numerically solving the equation for the scaled gap $x_S(H, L) = \frac{2}{9}$ based on the KT criterion (see below). Then, in order to accelerate the slow convergence of $H_c(L)$, the iterated fits taking account of the logarithmic correction were performed. On the other hand, it is widely recognized that the level-spectroscopy (LS) method provides an efficient way to treat the BKT transitions [10, 11]. Therefore, for its application, let us consider the system on Λ with M ($\to\infty$) rows in the x_2 direction of L (a multiple of three) sites in the x_1 direction wrapped on the cylinder and define the transfer matrix connecting the next-nearest-neighbour rows. Since Q is the most important conserved quantity in the transfer, we explicitly specify a block of the matrix as $\mathbf{T}_Q(L)$ and denote its eigenvalues as $\lambda_{p,Q}(L)$ or their logarithms as $E_{p,Q}(L) = -\frac{1}{2}\ln|\lambda_{p,Q}(L)|$ (p specifies a level). In the isotropic case, the smallest one corresponding to the ground state is in the block $Q_0 = 2L/3$ [3, 5]; we shall denote it and excitation gaps from it as $E_{g,Q_0}(L)$ and $\Delta E_{p,Q}(L) = E_{p,Q}(L) - E_{g,Q_0}(L)$, respectively. Then the conformal invariance provides direct expressions for the central charge c and a scaling dimension $x_{p,Q}$ in the critical system as $E_{g,Q_0}(L) \simeq Lf - \pi c/6L\zeta$ and $\Delta E_{p,Q}(L) \simeq 2\pi x_{p,Q}/L\zeta$. Here ζ ($=2/\sqrt{3}$) and f are the geometric factor for Λ and a free energy per site, respectively.

To determine the BKT point, Nomura pointed out the importance of logarithmic corrections in the renormalized scaling dimensions $x(l) = \Delta E(L)/(2\pi/L\zeta)(l = \ln L)$ [10]. Especially in the present case, the so-called $\mathcal{M}$-like operator plays an important role. Writing its dimension as $x_0(l)$, it has been discussed in [12] that the level-crossing condition, $x_0(l) = 4 - 9x_S(l)$, provides a finite-size estimate of the BKT point, where $x_S(l)$ is the dimension of S. Since these operators are described by ϕ, we can calculate their dimensions from excitation gaps found in the Q_0 block [12]. We perform the exact-diagonalization (ED) calculations of $\mathbf{T}_{Q_0}(L)$ for systems up to $L = 30$. In figure 2(a), we show the extrapolation of the finite-size estimates $H_c(L)$ to $L \to \infty$ using the least-squares fitting of the polynomial in $1/L^2$ (circles with a curve). For comparison, we also plot the finite-size estimations given in table 1 of [5] (diamonds). Then, we find that while our result, $H_c \simeq 0.5229 \pm 0.001$, is consistent with BN's estimation (the diamond with error bar), it is more accurate owing to the fast convergence of finite-size estimates, which is one of the benefits of using the LS method.

To see to what extent the string alignment is established on the upper side of H_c, it is interesting to observe the expectation value of the twist operator which has been discussed

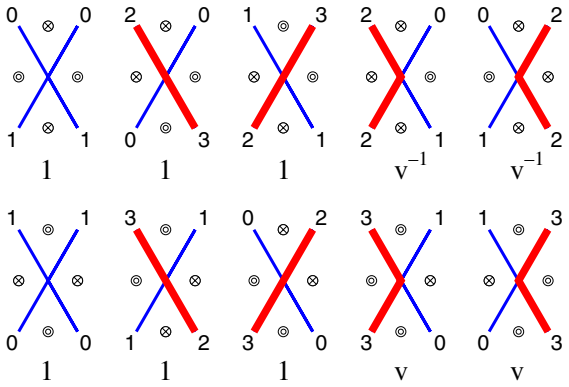

Figure 3. Vertices and weights. Thin (blue) and thick (red) lines are drawn in the same manner as figure 1(b). The mark ⊙ (⊗) on Λ shows the parallel (antiparallel) spins to the field. Numbers on four edges of each vertex denote four-state link variables τ_n.

in research on 1D quantum systems [13]. In the present case, it is given by $z(H) = \langle \exp[(6\pi \mathrm{i}/L) \sum_{j_1=1}^{L} j_1 N_{j_1,j_2}] \rangle$. This takes unit value for the completely ordered states with the $\sqrt{3} \times \sqrt{3}$ structure, while it is expected to be zero for the critical phase. In figure 2(b), we exhibit the numerical calculation results for finite-size systems up to $L = 27$. We find that $z(H)$ is real for all H, and zero at $H = 0$. Further, with the increase of H, $z(H)$ increases and converges to unity, which clearly reflects the ordering of the string alignment. In the inset, we provide the system-size dependence of $z(H)$ in the weak field region. Although the precise estimation of H_c is difficult from $z(H)$ [13], we can observe the crossing points (arrows in the inset) between different system-size data which are approaching the transition point. Thus, we can also recognize the existence of the phase transition from $z(H)$.

3. Results in the anisotropic case $\mu \neq 0$

As discussed in section 1, the anisotropy parameter μ controls the number of strings and brings about the PT transition for $H > H_c$, so the estimation of the incompressible region observed in the μ dependence of Q (or its density $\rho = Q/L$) is necessary. For this, we employ the density-matrix renormalization-group (DMRG) method [14] and estimate the μ–ρ curve from the finite-size-system data as $\mu \simeq [E_{g,Q+2}(L) - E_{g,Q}(L)]/2$ [7]. In order to treat the transfer matrix in our problem with DMRG, we use the vertex representation of the Boltzmann weight, which enables us to explicitly handle the number of strings. We define the vertex on each horizontal bond of Λ expressed as the crossing points of colored lines in figure 1(b). The details of the vertices and their weights are summarized in figure 3. The vertices with thin blue and thick red lines (the right eight) describe the strings coming from the south east or south west direction and going out to the north east or north west direction, whereas those with blue lines (the left two) play the role of a spacer between the strings. The magnetic field effect can be taken into account by giving the weight $v^{\pm 1} = \mathrm{e}^{\pm H/4}$ for the vertex having the excess of the parallel (antiparallel) spins to the field. Then, as defined in the figure, we assign a four-state link variable ($\tau_n = 0, 1, 2, 3$) on each edge of the vertex. Here note that, due to the ground-state condition of TAFIM, ten types of vertices have nonzero weights, but, for the case $H = 0$, the problem is described by a five-vertex model.

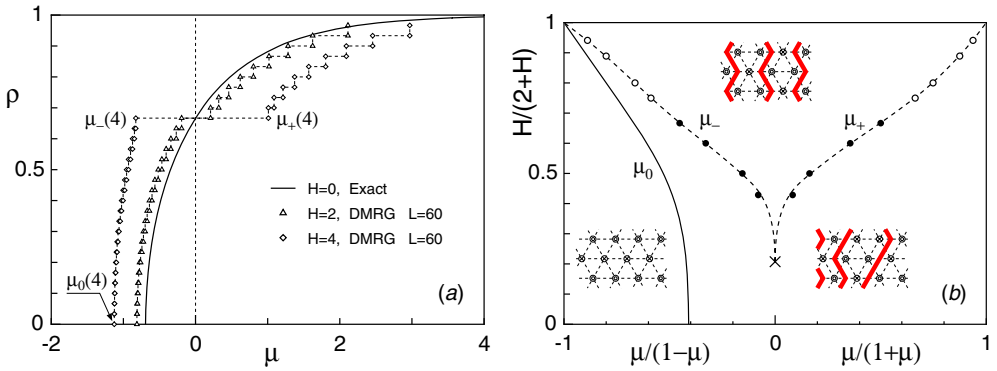

Figure 4. (a) The μ–ρ curves: marks with the dotted line show DMRG data, and the solid line exhibits the exact result at $H = 0$. The flat region with $\rho = \frac{2}{3}$ corresponds to the string-density plateau $[\mu_-(H), \mu_+(H)]$. $\mu_0(H)$ is the threshold below which the string is absent. (b) The ground-state phase diagram (typical configurations are also given). On the left of the solid curve $\mu_0(H)$, $\rho = 0$. The cross at $\mu = 0$ shows the BKT point obtained by the LS method. The filled (open) circles show estimates $\mu_\pm(H)$ by the DMRG (ED) method. Dotted curves give a guide to the eyes.

On the basis of the vertex representation, we construct the diagonal-to-diagonal transfer matrix of two layers $\mathbf{T}^{\mathrm{DMRG}}_{\{\tau_1\cdots\tau_{2L}\},\{\tau'_1\cdots\tau'_{2L}\}}$ depicted in figure 1(b). $\mathbf{T}^{\mathrm{DMRG}}$ is suitable for a renormalization process in DMRG, since it can be represented as a product of the local vertex weights carrying string number. However, instead of this benefit, the matrix becomes asymmetric, for which the definition of the reduced density matrix is not unique. For this issue, we employ the symmetric density matrix constructed from the right eigenvector of $\mathbf{T}_{\mathrm{DMRG}}$, and perform the finite-system-size DMRG calculations in the subspace of a fixed Q. In actual calculations, we have confirmed that the free energy value converges sufficiently within the base number $m = 64$ [14].

We show the data of the μ–ρ curve in figure 4(a). While, like the exact solid curve $\rho(\mu) = \arccos(1/2\mathrm{e}^{2\mu} - 1)/\pi$ for $H = 0$ [3], ρ is a smooth function of μ showing the compressive liquid state for $H \leqslant H_c$, there is the string-density plateau with $\rho = \frac{2}{3}$ for $H > H_c$ (in this plot, the top and the bottom of each step correspond to $(Q+2)/L$ and Q/L respectively). So, we can estimate the C–IC phase boundary lines from the edges of the plateau $\mu_\pm(H)$. In figure 4(b), we provide our phase diagram [12]. Here, the exact threshold $\mu_0(H) = -\ln[2\cosh(H/4)]$, below which the doubly degenerate vacuum of strings with $\rho = 0$ is realized (see figure 4(a)), is also given [15]. The cross at $\mu = 0$ shows the BKT point obtained by the LS method. For large H, we can use the ED data and the extrapolation formula $\mu_\pm(H, L) \simeq \mu_\pm(H) + \mathrm{constant}/L^2$ (open circles). For $H \lesssim 4$, assuming the square-root behaviour around the plateau, we estimate $\mu_\pm(H)$ from the ρ–μ curve obtained by DMRG. Then, we find that two PT-transition lines $\mu_\pm(H)$ seem to be terminated at the BKT point $(\mu, H) = (0, H_c)$. For $H \simeq H_c$, it is still difficult to determine the narrow plateau region corresponding to the exponentially small energy gap even by the use of the DMRG method. However, by combining the LS result and the DMRG data, we can provide a reliable phase diagram.

Lastly, it is worth pointing out that the magnetization process observed in the ground state of the $S = \frac{1}{2}$ frustrated spin chain system exhibits the plateau at $\frac{1}{3}$ of the saturation magnetization [16], and the plateau formation is described by the same field theory as the present one. The μ–ρ curve in figure 4(a) can be thus viewed as the magnetization curve observed in the 1D quantum spin system.

Acknowledgments

Numerical calculations were carried out on SX8 at YITP in Kyoto University. This work was supported by Grants-in-Aid from the Japan Society for the Promotion of Science.

References

[1] For example, Wannier G H 1950 *Phys. Rev.* **79** 357
[2] Stephenson J 1970 *J. Math. Phys.* **11** 413
[3] Blöte H W J and Hilhorst H J 1982 *J. Phys. A: Math. Gen.* **15** L631
[4] Nienhuis B, Hilhorst H J and Blöte H W J 1984 *J. Phys. A: Math. Gen.* **17** 3559
[5] Blöte H W J and Nightingale M P 1993 *Phys. Rev.* B **47** 15046
[6] Blöte H W J and Nienhuis B 1994 *Phys. Rev. Lett.* **72** 1372
[7] Noh J D and Kim D 1995 *Phys. Rev.* E **51** 226
[8] Pokrovsky V L and Talapov A L 1979 *Phys. Rev. Lett.* **42** 65
[9] Noh J D and Kim D 1994 *Phys. Rev.* E **49** 1943
[10] Nomura K 1995 *J. Phys. A: Math. Gen.* **28** 5451
[11] Otsuka H, Mori K, Okabe Y and Nomura K 2005 *Phys. Rev.* E **72** 046103
Matsuo H and Nomura K 2006 *J. Phys. A: Math. Gen.* **39** 2953
[12] Otsuka H, Okabe Y and Okunishi K 2006 *Phys. Rev.* E **73** 035105(R) and the references therein
[13] Nakamura M and Voit J 2002 *Phys. Rev.* B **65** 153110 and the references therein
[14] White S R 1992 *Phys. Rev. Lett.* **69** 2863
White S R 1993 *Phys. Rev.* B **48** 10345
[15] Lin K Y and Wu F Y 1979 *Z. Phys.* B **33** 181
[16] Okunishi K and Tonegawa T 2003 *J. Phys. Soc. Japan* **72** 479